Robust Tension Control of the Anchor Chain of the Ship Windlass under Sea Wind

Wangqiang Niu, Jianxin Chu, Wei Gu
Marine Technology & Control Engineering Key Laboratory,
Shanghai Maritime University, Shanghai, 200135, China
Email: wqniu@rin.shmtu.edu.cn

***Abstract*—Constant tension control of anchor chains is important for safety of moored ships. The core driving component of an anchor windlass system is an induction motor which is a multi-variables, coupled nonlinear system, and is difficult to control. To surmount this problem, a control scheme based on the inverse system method is introduced to linearize an induction motor into a decoupled linear system, and linear controllers are then designed to complete the control task. In addition, theoretical analysis based on the Lyapnov method is carried out to investigate the influence of the time-varying rotor resistance to the control scheme suggested. Both theoretical analysis and numerical simulations show this control scheme is able to keep anchor chains at desired tension under sea wind at a time-varying rotor resistance.**

***Index Terms*—anchor windlass, constant tension control, induction motor, inverse system, adaptive nonlinear control, time-varying rotor resistance**

I. INTRODUCTION

Ships are moored to the sea-bottom by the anchor system consisting of: anchor, chain, stoppers, chain locker and windlass [1]. Constant tension control of anchor chains is important for safety of moored ships. When strong sea wind is coming, the tension of an anchor chain might be greater than its maximum allowable value, the chain might be broken, and the ship might be blown away.

Constant tension control of anchor chains is to automatically adjust their length (loosened or tightened) to counteract the external disturbance from sea wind, wave and ocean currents.

The anchor windlass consists of induction motor, reduction gear and chain warehouse. The driving force from the windlass is generated by the induction motor, and the motor torque is adjusted automatically to control the tension of the anchor chain.

The induction motor is a multi-variables, coupled nonlinear system, and three control methods are developed recently: input-output linearization, energy shaping (passivity-based control), and backstepping design [2]. Compared to the last two methods, the linearization approach is engineer-oriented. Its idea is to use state feedback to linearize a nonlinear system. One of the linearization methods is the differential-geometric approach [3], which is mathematically complex and Lie derivatives are involved. Another linearization method is the inverse system approach [4-9], which use the concept of mapping, and is easy to master by engineers. In this study, the inverse system approach is used to linearize the windlass motor, and linear controllers are designed to fulfill constant tension control of an anchor chain under see wind.

In practice, the rotor resistance may have a ±50% variations around its rated value due to the rotor heating [3]. Marino et al. propose a nice adaptive scheme to deal with an unknown and constant rotor resistance using the geometric techniques [3]. Zhou & Han propose a complex adaptive scheme for a constant and unknown rotor resistance based on the inverse system method [10]. In this contribution, a detailed analysis is carried out to investigate the influence of the time-varying rotor resistance to the control performance of the inverse system method. It is found that the control scheme based on the inverse system method is able to keep the chain tension at the desired value under a time-varying rotor resistance. It is also found that the speed pathway and the torque pathway are independence of the rotor resistance, while the flux pathway is related to the rotor resistance. Theoretical analysis from the Lyapnov method shows that when the reference flux is a constant signal, the rotor flux is able to track its reference signal at a time-varying rotor resistance.

Simulated experiments are carried out to test the control scheme both at the non-adaptive case and the adaptive case. A step rotor resistance and a ramp rotor resistance are used in the adaptive case. The simulation shows that the control scheme based on the inverse system method is robust to a time-varying rotor resistance.

II. THE MODELS

A. The Anchor Windlass System

The tension of an anchor chain, H_{chain}, is described by:

$$H_{chain} = H_{windlass} + H_{wind}, \quad (1)$$

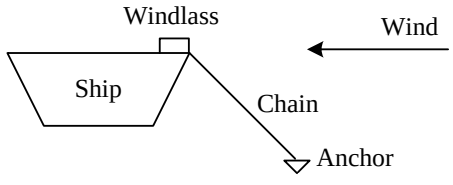

Figure 1. The anchor system.

doi:10.4304/jcp.5.4.631-637

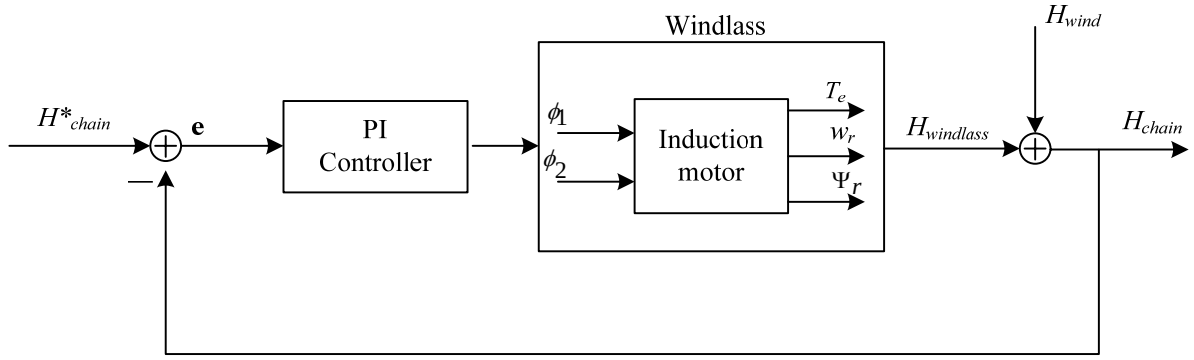

Figure 2. The constant tension control framework.

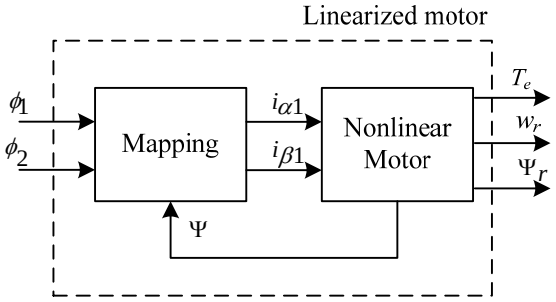

Figure 3. The inverse system linearization method.

where $H_{windlass}$ is the force from the windlass, and H_{wind} is the force generated by sea wind, Fig. 1 and 2. The wind acts on the ship, and the ship then acts on the anchor chain through the windlass system.

B. The Constant Tension Control Framework

The constant tension control framework is shown in Fig. 2. H^*_{chain}, the desired tension of the chain, is compared with the real tension, H_{chain}. The error signal, H^*_{chain} - H_{chain}, is sent to the controller. The controller generates the input signal of the windlass, and $H_{windlass}$ is generated to counteract the wind disturbance, H_{wind}.

C. The Induction Motor in the Windlass

The key part of the anchor windlass system is the induction motor. In this study, the motor is modeled mathematically, and other parts in the windlass are neglected.

In a two phase α, β representation of an induction motor, the dynamics is described by [2, 3, 5, 10, 11]:

$$\begin{aligned}
\frac{dw_r(t)}{dt} &= \frac{p_n^2 L_m}{JL_r}(\Psi_{\alpha 2}(t) i_{\beta 1}(t) \\
&\quad - \Psi_{\beta 2}(t) i_{\alpha 1}(t)) - \frac{p_n}{J} T_L \\
\frac{d\Psi_{\alpha 2}(t)}{dt} &= -\frac{1}{T_r}\Psi_{\alpha 2}(t) - w_r(t)\Psi_{\beta 2}(t) + \frac{L_m}{T_r} i_{\alpha 1}(t) \\
\frac{d\Psi_{\beta 2}(t)}{dt} &= -\frac{1}{T_r}\Psi_{\beta 2}(t) + w_r(t)\Psi_{\alpha 2}(t) + \frac{L_m}{T_r} i_{\beta 1}(t)
\end{aligned} \quad , \quad (2)$$

where w_r is the rotor speed; the subscripts 1 and 2 stand for stator and rotor; $\Psi_{\alpha 2}$ and $\Psi_{\beta 2}$ are the α and β components of the rotor flux; $i_{\alpha 1}$ and $i_{\beta 1}$ are the α and β components of input currents to the stator; L_r is the rotor inductance, L_m is the mutual inductance; R_r is the rotor resistance, $T_r = L_r/R_r$ is the time constant of the rotor; p_n is the number of the pole pairs; J is the moment of inertia of the rotor, and T_L is the load torque.

D. The Inverse System Linearization Method

The driving force of the motor is related to electromagnetic torque [11], T_e,

$$T_e(t) = \frac{L_m}{L_r}(\Psi_{\alpha 2}(t) i_{\beta 1}(t) - \Psi_{\beta 2}(t) i_{\alpha 1}(t)) . \quad (3)$$

The direct control of T_e is difficult because it is related to four variables: $i_{\alpha 1}$, $i_{\beta 1}$, $\Psi_{\alpha 2}$ and $\Psi_{\beta 2}$. The linearization method is adopted here to simplify the control problem.

By the theory of inverse system [5, 9], define two new input variables, $\phi_1(t)$ and $\phi_2(t)$, and one new output variable, $\Psi_r(t)$, Fig. 3.

$$\begin{aligned}
i_{\alpha 1}(t) &= -\frac{JL_r}{p_n L_m}\frac{\Psi_{\beta 2}(t)}{\Psi^2_{\alpha 2}(t) + \Psi^2_{\beta 2}(t)}\phi_1(t) + \\
&\quad \frac{T_r}{L_m}\frac{\Psi_{\alpha 2}(t)}{(\Psi^2_{\alpha 2}(t) + \Psi^2_{\beta 2}(t))^{1/2}}\phi_2(t) + \frac{1}{L_m}\Psi_{\alpha 2}(t) \\
i_{\beta 1}(t) &= \frac{JL_r}{p_n L_m}\frac{\Psi_{\alpha 2}(t)}{\Psi^2_{\alpha 2}(t) + \Psi^2_{\beta 2}(t)}\phi_1(t) + \\
&\quad \frac{T_r}{L_m}\frac{\Psi_{\beta 2}(t)}{(\Psi^2_{\alpha 2}(t) + \Psi^2_{\beta 2}(t))^{1/2}}\phi_2(t) + \frac{1}{L_m}\Psi_{\beta 2}(t) \\
\Psi_r(t) &= (\Psi^2_{\alpha 2}(t) + \Psi^2_{\beta 2}(t))^{1/2}
\end{aligned} \quad .(4)$$

Substitute (4) to (2-3), the new linearized system is described by:

$$\begin{aligned} \frac{dw_r(t)}{dt} &= \phi_1(t) - \frac{p_n}{J} T_L \\ \frac{d\Psi_r(t)}{dt} &= \phi_2(t) \\ T_e(t) &= \frac{J}{p_n}\phi_1(t) \end{aligned} \quad . \tag{5}$$

This new system has three features. (a). It is a 1st-order linear system; (b). The rotor speed and flux are decoupled, that is, the speed $w_r(t)$ is only related to $\phi_1(t)$, and the flux $\Psi_r(t)$ is only influenced by $\phi_2(t)$; (c). Electromagnetic torque $T_e(t)$ is linearly related to $\phi_1(t)$, thus, $\phi_1(t)$ is named the torque input, and $\phi_2(t)$ the flux input.

E. The Design of Linear Controllers

The decoupled linear system facilitates linear controllers to adjust the chain tension. Two linear PI controllers are designed, one for the torque pathway, the other for the flux pathway.

F. The Robust Tension Control

In practice, the rotor resistance R_r may have a $\pm 50\%$ variations around its rated value due to the rotor heating [3]. The control framework suggested above is analyzed for its robustness to the variations of the rotor resistance R_r.

Let $R_r(t)$ the real rotor resistance, R_r^* the rated rotor resistance, $T_r(t)$ the real time constant of the rotor, T_r^* the rated time constant of the rotor, $T_r^* = L_r / R_r^*$. Because $R_r(t)$ is an unknown parameter, R_r^* (T_r^*) is used to define the feedback variables, $i_{\alpha 1}$ and $i_{\beta 1}$.

$$\begin{aligned} i_{\alpha 1}(t) &= -\frac{JL_r}{p_n L_m}\frac{\Psi_{\beta 2}(t)}{\Psi^2_{\alpha 2}(t) + \Psi^2_{\beta 2}(t)}\phi_1(t) + \\ &\quad \frac{T_r^*}{L_m}\frac{\Psi_{\alpha 2}(t)}{(\Psi^2_{\alpha 2}(t) + \Psi^2_{\beta 2}(t))^{1/2}}\phi_2(t) + \frac{1}{L_m}\Psi_{\alpha 2}(t) \\ i_{\beta 1}(t) &= \frac{JL_r}{p_n L_m}\frac{\Psi_{\alpha 2}(t)}{\Psi^2_{\alpha 2}(t) + \Psi^2_{\beta 2}(t)}\phi_1(t) + \\ &\quad \frac{T_r^*}{L_m}\frac{\Psi_{\beta 2}(t)}{(\Psi^2_{\alpha 2}(t) + \Psi^2_{\beta 2}(t))^{1/2}}\phi_2(t) + \frac{1}{L_m}\Psi_{\beta 2}(t) \end{aligned} \quad . \tag{6}$$

Substitute (6) to (2-3), the new linearized system is described by:

$$\begin{aligned} \frac{dw_r(t)}{dt} &= \phi_1(t) - \frac{p_n}{J} T_L \\ \frac{d\Psi_r(t)}{dt} &= \frac{T_r^*}{T_r(t)}\phi_2(t) \\ T_e(t) &= \frac{J}{p_n}\phi_1(t) \end{aligned} \quad . \tag{7}$$

The speed equation and the electromagnetic torque equation in (7) are independent of $T_r(t)$. The elegant symmetry of (2, 3, 6) causes the complete counteraction of the terms which contain the parameter $T_r(t)$. Consequently, $w(t)$ and $T_e(t)$ are insensitive to the variations of the rotor resistance $R_r(t)$.

The variations of the rotor resistance $R_r(t)$ will influence the flux $\Psi_r(t)$ in (7), however, the whole flux pathway in the close-loop control framework in Fig. 2 is also insensitive to the variations of the rotor resistance $R_r(t)$. The reason is explained theoretically in succession.

The PI controller in the flux pathway is defined as

$$\begin{aligned} \phi_2(t) &= K_P e(t) + K_I \int e(t)dt \\ e(t) &= \Psi_r^*(t) - \Psi_r(t) \end{aligned} \quad , \tag{8}$$

where K_P is the proportional coefficient, K_I is the integrator coefficient, $\Psi_r^*(t)$ is the flux reference signal, and $e(t)$ is the flux error signal.

Let $V(t)$ be a Lyapnov function,

$$V(t) = \frac{1}{2}e^2(t) , \tag{9}$$

then

$$\frac{dV(t)}{dt} = e(t)\frac{de(t)}{dt} = e(t)\left(\frac{d\Psi_r^*(t)}{dt} - \frac{d\Psi_r(t)}{dt}\right) . \tag{10}$$

Let

$$\frac{d\Psi_r^*(t)}{dt} = 0 , \tag{11}$$

e.g., a constant flux reference signal, then

$$\begin{aligned} \frac{dV(t)}{dt} &= -e(t)\frac{d\Psi_r(t)}{dt} \\ &= -e(t)\frac{T_r^*}{T_r(t)}(K_P e(t) + K_I \int e(t)dt) \\ &= -\frac{T_r^*}{T_r(t)}[K_P e^2(t) + K_I e(t)\int e(t)dt] < 0 \end{aligned} \quad . \tag{12}$$

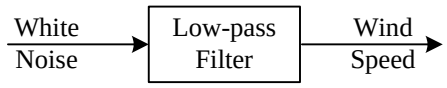

Figure 4. The sea wind simulation model.

Because $V(t)$ is a bounded L^2 signal with bounded derivative $\dot{V}(t)$, by Barlalat lemma [3, 10, 12], it follows that

$$\lim_{t \to \infty} \| V(t) \| = 0 , \tag{13}$$

i.e., the flux $\Psi_r(t)$ is able to track asymptotically its reference signal $\Psi_r^*(t)$.

In short, the variations of the rotor resistance $R_r(t)$ will not influence the key variables, $w(t)$, $\Psi_r(t)$ and $T_e(t)$, that is, the tension control framework in Fig. 2 is robust to the variations of the rotor resistance $R_r(t)$.

G. The Sea Wind Model

Sea wind consists of two parts, one is mean wind whose speed is unchanged for 10 to 60 minutes, the other is turbulent wind whose amplitude and direction are changed randomly [12, 13].

Sorensen et al. used following equation to describe the force duo to wave, ocean currents and wind [14],

$$\frac{db(t)}{dt} = -T^{-1} b(t) + Ew(t) , \tag{14}$$

where $b(t)$ is the force, T is the time constant, $w(t)$ is a zero-mean bounded disturbance, and E is the scaling coefficient.

Perform the Laplace transform on (14), the result is

$$\frac{b(s)}{w(s)} = \frac{T}{Ts+1} , \tag{15}$$

where $b(s)$ and $w(s)$ are the Laplace transform of $b(t)$ and $w(t)$, respectively. Equation (15) is a low-pass filter. In this study, the wind is simulated by a white noise passing a low-pass filter, Fig. 4. The mean of the white noise describes the mean wind, and the variance of the white noise represents the turbulent wind.

III. The Simulation Results

Numerical simulation experiments are employed to test the control scheme introduced previously. The simulation parameters are described firstly, and then the simulation results are explained. The non-adaptive case with a constant rating rotor resistance is introduced firstly, and then the adaptive case with a step and a ramp rotor resistance is depicted. The simulation tool is Matlab/Simulink (Mathworks Inc, Natick, MA).

A. The Parameters of the Models

The simulated induction motor of the windlass has a power rating of 15 kW, a speed rating of 220 rad/s, and a flux rating of 1.3Wb, for other parameters[6], see Table I.

TABLE I.
PARAMETERS OF THE INDUCTION MOTOR

Parameter	Value	Unit
L_r	0.0699	H
L_m	0.068	H
R_r	0.15	Ω
T_r	0.466	s
p_n	1	-
J	0.0586	kgm^2

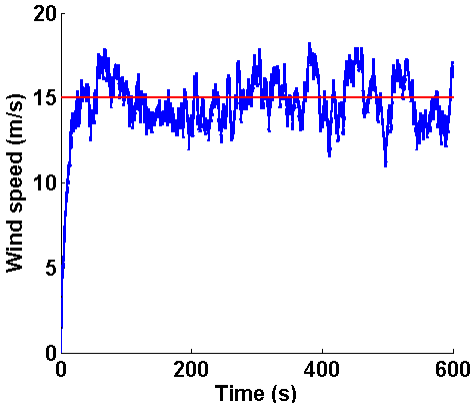

Figure 5. The simulation of sea wind.

When the mean wind is 15 m/s, the wind Davenport power spectrum has a peak value at 0.06 rad/s of the angle frequency, w. When w is 0.1 rad/s, the wind spectrum is a factor of 0.707 of its peak [13]. For $T=2\pi/w \approx 60$ s, the time constant of the low-pass filter is set to 60 s. The input white noise has a mean of 15, and a variance of 15^2.

Two linear PI controllers for the torque and flux pathways have same parameters, the proportional coefficient is set to 900, and the integrator coefficient is set to 90.

B. The Sea Wind

The simulation of the wind speed is shown in Fig. 5. The wind has a mean speed of 15 m/s, and fluctuates between 12 and 18 m/s. The main fluctuating period is 16 s. Sorensen et al. showed a segment of wind speed measured at North Sea, Europe [14]. The wind in their Fig. 11 has a mean velocity of 22 m/s, varies between 18 and 26 m/s, its main fluctuating period is 25 s. Compared with their data, the simulation in this study is acceptable.

The time constant of the low-pass filter is 60 s, and thus the simulated wind takes roughly 60 s to get its shape.

C. The Constant Tension Control of the Windlass Chain – the Non-adaptive Case

The induction motor described by (2) has a constant rotor resistance with a rating value of 0.15 Ω in this simulated experiment.

1) The tension of the anchor chain

The desired tension of the anchor chain is set to 10 kN, and the wind disturbance is randomly varying around 5 kN. As shown in Fig. 6, the real chain tension is kept at 10 kN, as desired. The output force of the windlass is symmetric with the wind disturbance about the line of 5

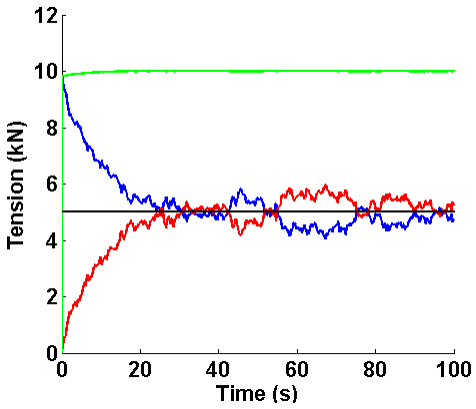

Figure 6. The tension output of the anchor system at the non-adaptive case. The green, blue, and red lines are the chain tension, the output force of the windlass, and the wind disturbance, respectively.

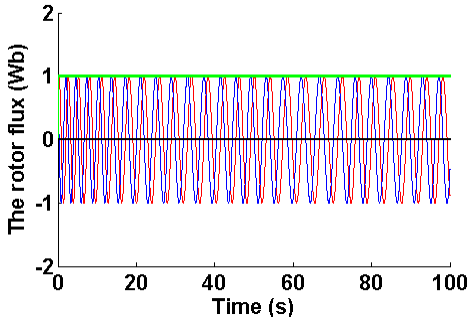

Figure 7. The rotor flux at the non-adaptive case. The green, red, and blue lines are the flux $\Psi_r(t)$, $\Psi_{\alpha 2}$, and $\Psi_{\beta 2}$, respectively.

kN, and thus their sum would result in a constant chain tension of 10 kN.

The key physical states of the induction motor of an anchor windlass are the stator current, the rotor flux, and the rotor speed. They are described subsequently.

2) The stator current

Input currents to the motor stator, $i_{\alpha 1}$ and $i_{\beta 1}$, are shown in Fig. 8. Their phase is $\pi/2$ depart, that is they are a sine-cosine pair in the time domain. This is the basic characteristic of a two phase α, β reference frame [11]. Their periods are increased gradually from 3 s to 4 s, and their amplitudes are roughly 25 A.

The initial transient fluctuation is the transition process. The amplitudes of $1000A$ are caused by the saturation device whose saturation value is set to $1000A$. Why the stator currents show these features is a challenging question which will be investigated in the future.

3) The rotor flux

The rotor fluxes, $\Psi_{\alpha 2}$ and $\Psi_{\beta 2}$, show characteristics similar to the stator currents, $i_{\alpha 1}$ and $i_{\beta 1}$, Fig. 7. They are also a sine-cosine pair, and their periods are also increased gradually from 3 s to 4 s. The Flux $\Psi_r(t)$ is set to 1 Wb, and a PI controller is adopted to keep it at its expected value.

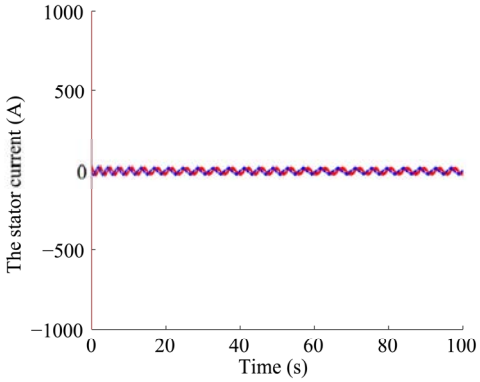

Figure 8. The stator currents at the non-adaptive case. The red and blue lines are the α and β components, respectively.

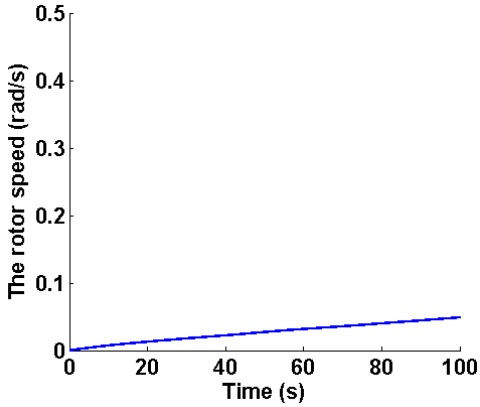

Figure 9. The rotor speed at the non-adaptive case.

4) The rotor speed

The rotor speed, w_r, is close to 0 rad/s, Fig. 9. The steady increase to 0.05 rad/s might be caused by some integrator modules.

D. The Constant Tension Control of the Windlass Chain – the Adaptive Case

The adaptive characteristics of the control framework suggested above are tested by a step and a ramp rotor resistance.

1) The step rotor resistance

The induction motor has a constant rotor resistance with a rating value of $0.15\,\Omega$ during the first 50s, and the rotor resistance steps to a 150% rating value at the tick of 50s and keeps at this value during the last 50s.

The chain tension is still kept at the desired value of 10 KN when the rotor resistance steps to a 150% rating value. The output force of the windlass is same to the non-adaptive value, comparing Fig. 6 and 10. The rotor speed is still close to 0 rad/s, comparing Fig. 9 and 11.

The step variation of the rotor resistance results in a decrease of the damp coefficient of the flux dynamics in the motor system (2), and consequently, the oscillating frequencies of the rotor flux and the stator current are increased. In Fig. 12, the rotor flux $\Psi_{\alpha 2}$ changes its oscillating period from 4s to 3s at the tick of 50s. For simplicity, the dynamics of the stator current is not shown

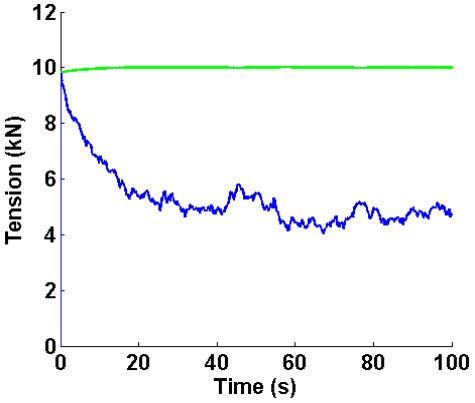

Figure 10. The tension output of the anchor system at the adaptive case with a step rotor resistance. Conventions as in Fig. 6.

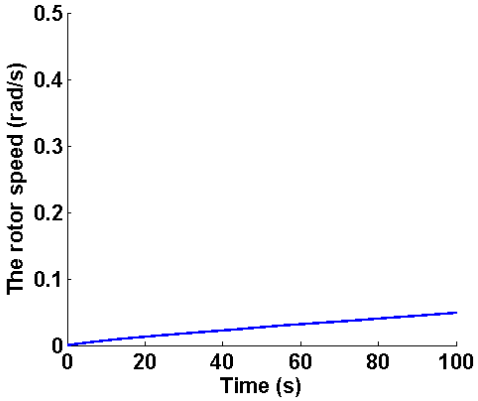

Figure 11. The rotor speed at the adaptive case with a step rotor resistance.

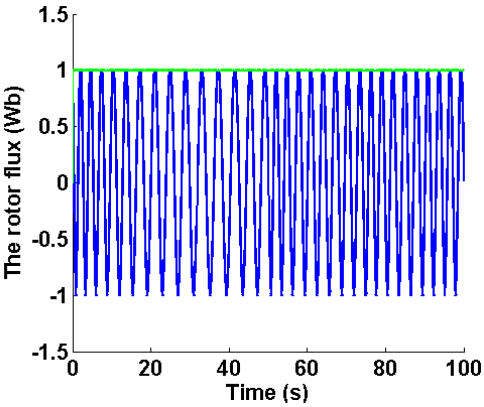

Figure 12. The rotor flux at the adaptive case with a step rotor resistance. Conventions as in Fig. 7.

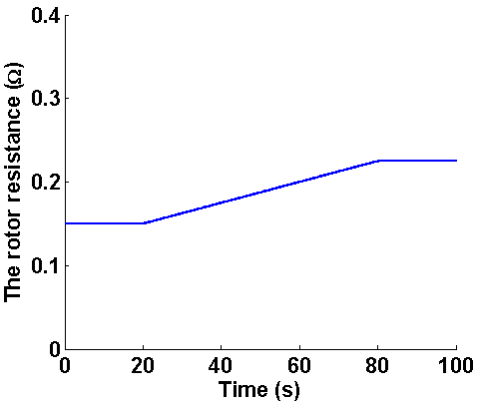

Figure 13. The ramp rotor resistance at the adaptive case.

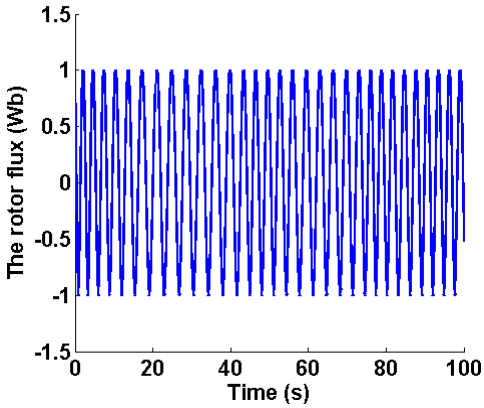

Figure 14. The rotor flux at the adaptive case with a ramp rotor resistance. Conventions as in Fig. 7.

here, and they also show characteristics similar to the rotor flux $\Psi_{\alpha 2}$.

2) The ramp rotor resistance

The induction motor has a constant rotor resistance with a rating value of 0.15 Ω during the first 20s, and the rotor resistance increases gradually during the period of 20s to 80s, and it reaches a 150% rating value at the tick of 80s and keeps at this value during the last 20s, Fig. 13.

The chain tension, the output force of the windlass, and the rotor speed are all similar to the non-adaptive version (data not shown).

In Fig. 14, the rotor flux $\Psi_{\alpha 2}$ changes gradually its oscillating period from 4s to 3s during the interval from 20s to 80s due to the variations of the system damp. For simplicity, the dynamics of the stator current is not shown here, and they also show characteristics similar to the rotor flux $\Psi_{\alpha 2}$.

In short, these two experiments show that the control scheme is able to keep anchor chains at desired tension when the rotor resistance has a step change or a ramp change, that is, it is robust to the variations of the rotor resistance.

IV. Conclusion

The induction motor of the anchor windlass system is a multi-variables, coupled nonlinear system, and is the biggest obstacle to the constant tension control of the anchor chain. To overcome this barrier, the inverse system method is adopted to transform the induction motor into a decoupled linear system, and thus linear controllers are designed. The robustness of the control scheme to a time-varying rotor resistance is further analyzed. Both theoretical analysis and numerical simulations show this control scheme is able to keep the anchor chain at desired tension under sea wind at a time-varying rotor resistance.

Acknowledgement

J. Chu and W. Gu acknowledge the financial support of National Key Technology R&D Program Funded by Ministry of Science & Technology of China (No. 2007BAF10B03, No. 2007BAF10B05), and Shanghai

Sciences & Technology Committee under Grand No. 08DZ1202500 (08DZ1202502). W. Niu acknowledges the financial support of Special Science and Technology Research Funds for Shanghai Universities and Colleges to Select and Foster Excellent Young Teachers (No. SHS08036).

REFERENCES

[1] A. Munitic, M. Orsulic, M. Krcum, and J. Dvornik, "System dynamic simulating modelling of driving system "Anchor windlass driven by asynchronous motor" (bsvpam)," in *Esm 2003: 17th european simulation multiconference - foundations for successful modelling & simulation*, D. AlDabass, Ed. Ghent: Scs Europe, 2003, pp. 520-525.

[2] D. G. Taylor, "Nonlinear control of electric machines: An overview," *Control Systems Magazine, IEEE*, vol. 14, pp. 41-51, 1994.

[3] R. Marino, S. Peresada, and P. Valigi, "Adaptive input-output linearizing control of induction motors," *IEEE Transactions on Automatic Control*, vol. 38, pp. 208-221, 1993.

[4] X. H. Zhang, "Adaptive inverse decoupling control of induction motors," in *Proceedings of 2005 chinese control and decision conference, vols 1 and 2*, S. Y. Zhang, Z. G. Han, and F. Wang, Eds. Shengyang: Northeastern University Shengyang, 2005, pp. 401-405.

[5] J. R. Cao, L. Yu, and Y. B. Xie, "Decoupling and vector control of induction motor," *Journal of Xi'an Jiaotong University*, vol. 34, pp. 71-75, 2000 (in Chinese).

[6] X. H. Zhang, X. Z. Dai, D. J. Lu, and J. Q. Shen, "A decoupling control method based on inverse system theory for induction motor drives," *Electric Drive*, pp. 28-31, 2001 (in Chinese).

[7] Y. Zhou, H. Q. Zhu, and T. B. Li, "Decoupling control of magnetically levitated induction motor with inverse system theory," in *Ipemc 2006: Ces/ieee 5th international power electronics and motion control conference, vols 1-3, conference proceedings*. New York: Ieee, 2006, pp. 1953-1957.

[8] J. B. Wu, Y. K. Sun, X. F. Liu, L. Zhang, G. H. Liu, and J. Q. Chen, "Decoupling control of radial force in bearingless switched reluctance motors based on inverse system," in *Wcica 2006: Sixth world congress on intelligent control and automation, vols 1-12, conference proceedings*. New York: Ieee, 2006, pp. 1100-1104.

[9] C. W. Li and Y. K. Feng, *Inverse system method for multivariable control systems* Beijing: Tsinghua University Press, 1991 (in Chinese).

[10] R. Zhou and Z. J. Han, "Adaptive control scheme of induction motors with unknown rotor resistance," *Journal of Tsinghua University (Sci & Tech)*, vol. 38, pp. 98-101, 1998 (in Chinese).

[11] B. S. Chen, *Automatic control system of electric drive*, 3rd ed. Beijing: China Machine Press, 2003 (in Chinese).

[12] T. I. Fossen, *Guidance and control of ocean vehicles* Chichester: John Wiley and Sons Ltd., 1994.

[13] Z. Shi, X. L. Yao, and X. P. Yu, *Vehicle control systems*. Beijing: Tsinghua University Press, 2008 (in Chinese).

[14] A. J. Sorensen, J. P. Strand, and T. I. Fossen, "Thruster assisted position mooring system for turret-anchored fpsos," presented at Control Applications, 1999. Proceedings of the 1999 IEEE International Conference on, 1999.

Wang-Qiang Niu received the M.S. degree from Northwestern Polytechnical University, Xi'an, China, in 2004 and the Ph.D. degree from Shanghai Jiao Tong University, Shanghai, China, in 2008.

Since June 2008, he is a Lecturer at Shanghai Maritime University, Shanghai, China. His research interests include nonlinear guidance and control of ships.

Jianxin Chu received the B.S. and M.S. degrees in engineering from Dalian Maritime University, Dalian, China, in 1982 and 1990, respectively.

Since 1999, he has been a Professor at Shanghai Maritime University, Shanghai, China. His research interests include fault detection and diagnosis, power electronics, and electrical driving.

Wei Gu received the B. Eng. and Ph. D degrees from Shanghai Maritime University, Shanghai, China, in 1982 and 2008, respectively.

He is a teacher at Shanghai Maritime University since 1982, and a professor at Shanghai Maritime University since 1997. He is the director of the Key Lab. of Marine Technology and Control Engineering of China Communication Ministry. His research interest is: marine information control technology.